Available online at www.sciencedirect.com
SCIENCE DIRECT®
Advances in Space Research 34 (2004) 727–733
ADVANCES IN SPACE RESEARCH (a COSPAR publication)
www.elsevier.com/locate/asr

Trace gas column retrieval – an error assessment study for GOME-2

R. de Beek *, M. Weber, V.V. Rozanov, A. Rozanov, A. Richter, J.P. Burrows

Institute of Environmental Physics, University of Bremen, FB-1, D-28334 Bremen, Germany

Received 6 January 2003; received in revised form 16 June 2003; accepted 19 June 2003

Abstract

As a follow-on of the successful GOME instrument aboard ERS-2 the GOME-2 series is planned to operate on METOP satellites after 2005. Focussing on meteorological applications GOME-2 is designed to measure the total column and profiles of atmospheric ozone and the distribution of other key atmospheric constituents like BrO and NO_2. The main differences to Global Ozone Monitoring Experiment (GOME) are the higher spatial resolution of 40×80 km^2 in combination with a larger swath width of 1920 km. In this study potential error sources have been analysed most relevant for high viewing angles or small ground pixel sizes as applicable to GOME-2. Instrumental and atmospheric error sources have been identified with respect to basic signal-to-noise errors based upon an instrument model and full-spherical atmospheric radiative transfer simulations. Potential error sources such as the reflectance of the atmosphere, refraction, bi-directional surface reflection, spatial aliasing effects due to inhomogeneities of the scene, and spectral resolution (undersampling, slit width) have been investigated. Effects due to changes in instrumental design, e.g. read-out time, slit width and spectral sampling, have been taken into account. Error sources identified as most significant for trace gas column retrieval are spectral signature in the diffuser plate reflectivity, sun-glint effects, undersampling residuals, and noise. An overview of the study results and conclusions for future GOME-2 retrieval and instrumental designs are presented.

1. Introduction

The METOP satellite series is scheduled for 15 years of operation. On board of each of the three satellites will be the nadir viewing double monochromator spectrometer GOME-2, which is the successor of the Global Ozone Monitoring Experiment GOME (Burrows et al., 1999a).

GOME-2 has an optical layout, which is almost identical to the GOME design. Light scattered by and reflected from the atmosphere and the ground enters the instrument via scan mirror, telescope, and entrance slit. It is then predispersed and separated into four channels by prisms and a dichroic filter. Each channel has a diode array detector having 1024 spectral pixels. s- and p-polarised light are generated by the predisperser prism system and are detected by separate broadband polarization measurement units. The scan mirror can also point to the calibration unit, which comprises a sun-view port, a spectral line source and, in contrast to GOME, an additional white light source for improved radiometric calibration. Compared to GOME, GOME-2 uses a broader swath width and at the same time smaller footprint array resulting in higher spatial resolution, and has an improved polarization detection system (Callies et al., 2000; Hartman et al., 2001).

GOME-2 has an integration time of 0.1875 s and a mean spatial resolution of 80×40 km^2. The read-out time of the detector arrays is 46.9 ms, which is relatively large compared to the integration time. GOME-2 gathers 24 radiance spectra during one across-track scan of 1920 km, providing global coverage within 2 days. In contrast, the GOME-design enables only three radiance spectra in 4.5 s scanning across-track from east to west, resulting in a spatial resolution of 320×40 km^2 with a read-out-time of 93 ms.

With several changes in design and operation of the new GOME-2 spectrometer the question arises how these changes effect trace gas retrievals. To answer this, a study has been initiated and funded by EUMETSAT, mainly comprising an ozone profile retrieval error analysis performed by Rutherford Appleton Laboratory

* Corresponding author. Tel.: +49-421-218-4475: fax: +49-421-218-4555.
E-mail address: ruediger.de_beek@iup.physik.uni-bremen.de (R. de Beek).

0273-1177/$30 © 2004 COSPAR. Published by Elsevier Ltd. All rights reserved.
doi:10.1016/j.asr.2003.06.042

(RAL, Oxfordshire, UK) and trace gas slant column retrieval error analyses covered by our institute (Kerridge et al., 2002). This paper does not represent a complete DOAS sensitivity and error study. Only those aspects which are strongly dependent of the instrumental design and operation have been investigated.

2. Error analysis

For the error analysis, GOME-2 earthshine radiances have been simulated using the radiative transfer model (RTM) SCIATRAN (former GOMETRAN (Rozanov et al., 1997)). SCIATRAN is capable of simulating multiple scattered radiance in pseudo-spherical as well as in full-spherical mode (Rozanov et al., 2001) at arbitrary viewing angles. Another relevant feature is the Ring modeling capability (Vountas et al., 1998). The spectral range covered is adopted to SCIAMACHY spectral range (220–2385 nm), which encompasses the GOME-2 spectral range.

In order to be representative for zonal and seasonal atmospheric variability, model radiances have been simulated for 12 geo-temporal scenarios according to GOME-2 geometries, spanning a diverse range of observing conditions, including several surface albedos (typically 0.05 and 0.8). Each of the scenarios covered 24 ground pixels of one across-track forward-scan. Ground pixel radiances have been simulated by averaging over 10 of 240 line-of-sight zenith angles (LOS) for each modeled observation. Most of the retrievals have been covered by a DOAS type algorithm (Platt and Perner, 1980; Eisinger, 1998), which uses absorption cross-sections and a low-order polynomial to account for broadband spectral scattering features, both fitted to the measured optical depth spectrum (log(atmospheric radiance/solar irradiance)) to achieve trace gas slant column densities.

The simulated spectra have been used to retrieve trace gas slant columns, first un-corrupted spectra to give the "perfect-fit" slant column and then corrupted by simulated error patterns to estimate percentage errors relative to the perfect-fit result. However, for some analyses, linear mapping of the error covariance matrix has been used. Signal-to-noise ratio (SNR) error budgets have been used as a reference to evaluate all other errors. For spectral noise simulations a GOME-2 instrument model has been used (Kerridge et al., 2002). For the case of opening the instrumental entrance slit considered, it has been assumed that the intensity increases linearly with slit width, SNR has been adapted accordingly.

As an example, Fig. 1 shows differential optical depth spectra of interfering trace gas species including Ring structures and the noise level in the fitting window used for NO_2 retrievals. Computations were made for April, 75°N. Besides NO_2, O_4 and O_3 cross-sections were included in the fit, the latter measured at two different temperatures. For most applications, cross-sections measured on-ground using the GOME flight model (GOME-FM) have been used (Burrows et al., 1998, 1999b). It can be seen that the Ring spectrum has the largest spectral features. In this particular case, the 1-sigma noise level is large compared to trace gas structures. However, for the biomass burning case (July, 5°N) where tropospheric NO_2 is present, the absorption structure is much larger.

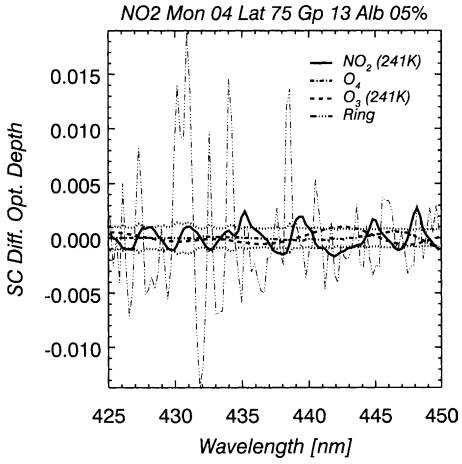

Fig. 1. Slant column (SC) differential optical depths and Ring spectrum as fitted for the NO_2 fitting window considered. 1-σ noise level is indicated by dots. Scenario April latitude 75°N, solar zenith angle 65°, stratospheric NO_2 only.

The dominance of O_3 in the UV window (325–335 nm) is demonstrated by Fig. 2. The Ring spectrum has still large structures, BrO and NO_2 spectral structures are below the noise level and are small compared to O_3 absorption structures.

The slant column density of O_3 is determined by the sum of fitted slant columns for each of the two ab-

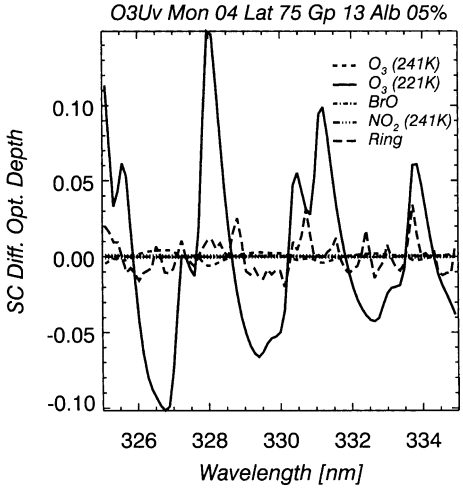

Fig. 2. As Fig. 1 but for O_3 fitted in the UV window (SC: slant column).

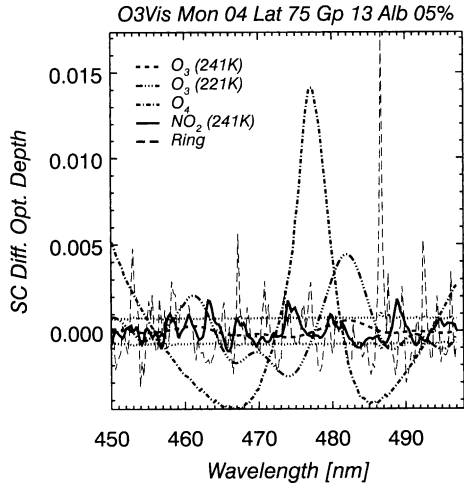

Fig. 3. As Fig. 1 but for O_3 fitted in the visible window (SC: slant column).

sorption cross-sections measured at 221 and 241 K. Which of both cross-sections is the dominant one varies depending on the ozone weighted mean temperature of the scenario used.

Accurate detection of O_3 in the visible window (Fig. 3) is more challenging due to significantly lower O_3 absorption as compared to the UV. Correlations with H_2O (not shown) and O_4 can effect the retrieval. Spectral structures due to the dichroic filter strongly interfere with O_3 around 470 nm, which can have large effects (de Beek, 2002). Errors for O_3 are an order of magnitude larger when fitted in the visible (450–497 nm) than in the UV. Due to less interference of molecular scattering in the visible compared to the UV spectral range, at large solar zenith angles the visible window might be of interest as source of additional information. However, such investigations are beyond the scope of this study.

A list of error sources considered in this study is given in Table 1, e.g. the SNR issue driven by an integration time of 0.1875 s per ground pixel, which is much shorter than for GOME (1.5 s).

Spatial aliasing spectral effects arise due to continuously scanning over an inhomogeneous ground scene, i.e. different detector pixels that are read out at different times observe different scenes and clouds. Depending on the structure, e.g. of a cloud field, various spectral signatures can occur having high and low frequencies. Correlations with trace gas signatures are therefore possible. Simulations have been made according to a representative set of Landsat-7 images (Kerridge et al., 2002).

Effects of RTM assumptions, relevant at Larger LOS angles, as well as bi-directional reflection distribution simulations have been investigated, the latter also in conjunction with ocean glint effects. In addition geolocation and pointing inaccuracies of the METOP platform are potential sources of errors.

Table 1
Overall error budget: Maximum and mean (brackets) error budgets obtained for each slant column retrieval error considered in the study

Category	Error Type	Trace gas			
		O3	O3 VIS	NO2	BrO
Basic SNR (IT=0.1875s)		<0.5% (0.3%)	<5% (3%)	<30% (15%)	<60% (30%)
Polarisation error		<0.4%			
Diffuser plate		0.3%	?	50%	70%
Spatial aliasing		0.2%		<2%	<1%
Spectral Resolution	Defocusing (1/2)*	0.3 %	3%	18%	35%
(*basic SNR included)	Open slit (1/2)*	0.2%	2%	11%	25%
	Interpolation (1/2)	-0.3%	-0.2%	-2%	25%
	Interpolation (1/0.8)	0.1%	1.6%	-20%	<-100%
	Interpolation (1/1.1)	0.0%	0.2%	-3%	-40%
RTM assumption	PS vs Spherical w/ refraction	<1%	<1%	<1%	<1%
	Spherical w/o refraction	<0.3%	<0.2%	<0.5%	<1%
	Spherical vs PS GRD	<1%		<1%	<1%
	Spherical vs PS TOA	<4%		<6%	<5%
BRDF		<0.3%	<3%	<2%	<3%
Pointing accuracy		<0.5%		<1%	<0.5%

Light-shaded are values in the same order of magnitude as for SNR, dark-shaded values are significantly larger than SNR errors. For reduction in spectral resolution by defocusing or open-slit, error budgets are given for a slit function having twice the nominal width. For interpolation, additionally ratios of 1/0.8 (strong under-sampling) and 1/1.1 with respect to the nominal spectral resolution are considered (see ratios in brackets). RTM simulations are performed in spherical and pseudo-spherical (PS) geometry, the latter for geometrical angles (solar zenith angle, line-of-sight and relative azimuth) valid for ground (GRD) and top-of-atmosphere (TOA) geometry.

Another error source for trace gas column retrievals is the differential spectrum produced by the diffuser plate interferring with absorption structures. This error is significant for aluminium diffuser plate material, that is also used by GOME and SCIAMACHY. A new quasi-volume-diffuser has been tested. Investigations about potential benefits to GOME-2 are on-going and an extension phase of the study is currently covering this topic.

Another potential error source, besides SNR errors and diffuser plate structures, is the spectral resolution issue that includes interpolation errors from Doppler-shift and under-sampling.

In the following the SNR error budget and the spectral resolution issue are described in more detail. An overview of maximum and mean error budgets achieved for all error sources investigated is summarised in Table 1.

3. Basic SNR errors

Errors for NO_2 due to noise assuming 0.1875 s integration time are shown in Fig. 4 as a function of ground pixel ranging from East to West. At 55°N and 5°N, errors are larger (up to 18%) due to smaller NO_2 slant paths at lower solar zenith angles. A slant path effect can also be seen for different LOS. Errors decrease for easterly and westerly viewing angles. The asymmetry of error pattern with respect to nadir viewing (ground-pixels 12/13) comes from the sphericity accounted for in the simulations. For the DOAS retrieval, the transformation from slant column to vertical column densities is done by multiplication with the inverse of the air-mass factor. Errors due to e.g. inconsistencies between model and measurement parameters, and a-priori climatology used in the air-mass factor calculations have not been explicitly covered by this study.

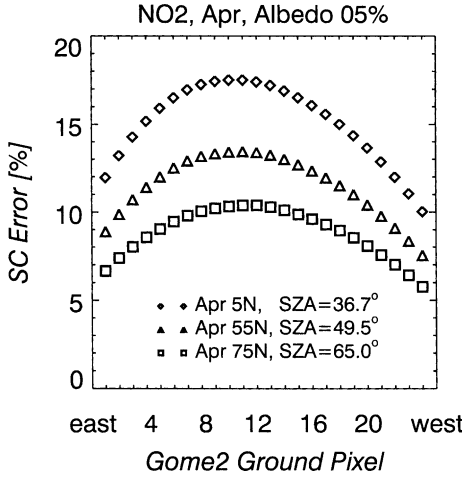

Fig. 4. NO_2 slant column DOAS retrieval: Errors due to noise, each for a given GOME-2 ground pixel, scanned from East to West viewing direction. At 55°N and 5°N, errors are larger due to less NO_2 and smaller slant paths (smaller SZA). In easterly and westerly viewing directions errors decrease due to increasing slant paths. The asymmetry with respect to nadir viewing (ground-pixels 12/13) points at the sphericity accounted for in the simulations.

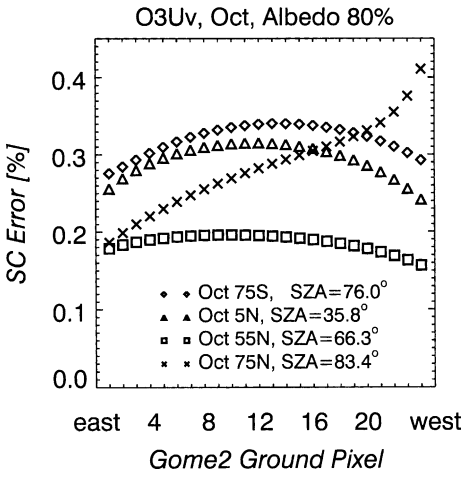

Fig. 5. Similar to Fig. 4 for O_3 for October: Sphericity, effects are noticable especially for 75°N latitude, were the instrument points westerly to the night terminator detecting low signals.

Fig. 5 shows results for O_3 in the UV in October; errors are small as expected. Again the sphericity shows up, particularly, at 75°N latitude, where the instrument points to the night terminator in the west direction, where low signals are detected. Generally, the retrieval accuracy is determined by the balance between the strength of trace gas signatures (density of molecules and light path) and SNR.

4. Reduction of spectral resolution

Oversampling according to the Nyquist theorem requires that the ratio of the slit function width over the spectral sampling interval (sampling ratio) is larger than two. The smaller the FWHM (full-width-at-half-maximum) the larger the spectral absorption features get. On the other hand interpolation errors due to spectral shifts, e.g. Doppler-shift, can get larger in this case. The Doppler-shift arises due to the relative motion of the instrument towards the sun in solar measurement mode in contrast to measurements of the earthshine radiance, where the field-of-view direction is perpendicular to the spacecraft motion. For the case of under-sampling, where the sampling ratio is below two (slit function FWHM is below two spectral pixel width) these interpolation errors would be enhanced (Roscoe et al., 1996).

Spectral error patterns due to interpolation errors after Doppler-shift corrections have been simulated using a highly resolved and sampled solar irradiance spectrum Irr_{hr} (Kurucz et al., 1984) and various slit functions (see e.g. Chance, 1998). Simulation starts by convolution of Irr_{hr} with the slit function of interest

(assumed gaussian). Irradiances are then assigned to the GOME-2 radiance wavelength grid, giving Irr_{og}, defined on the original wavelength grid, and the Doppler-shifted wavelength grid, giving Irr_{ds} (Doppler-shift is taken to be −0.008 nm, thus a shift of 0.008 nm as described is appropriate). After back-interpolation of Irr_{ds} onto the original wavelength grid, giving Irr^{bi}_{og}, the spectral interpolation error pattern is determined from the ratio lrr^{bi}_{og}/lrr_{og}. Of course, back-interpolation corrections in real world require exact knowledge of the shift at hand. The spectral interpolation error pattern can be directly fitted in a DOAS type manner to obtain the trace gas slant column fit error. Fig. 6 shows these errors as percentage errors with respect to perfect fit slant columns for four different scenarios. Sampling ratios between 1.6 (strongly under-sampled) and 4.0 have been used (one spectral pixel has been taken to cover 0.12 nm in Channel 2 and 0.24 nm in Channel 3).

Interpolation errors for trace gas slant columns depend on spectral sampling, spectral resolution, spectral shift, the correlation between the spectral error pattern and the fitted absorption cross-section, and on the absolute strength of the spectral error pattern relative to those of the absorption cross-sections, measured e.g. by root-mean-square values. The shape of the interpolation error pattern also depends on the specific values of the original wavelength grid of reference. Therefore, considering one specific spectral shift, the behaviour of the error as a function of FWHM is relatively complex and specific to the situation and can be highly variable, although the mean interpolation errors decrease with decreasing spectral resolution. For ozone, slant column errors increase with increasing FWHM of the slit function. For BrO, errors are large (around 40%) and highly variable.

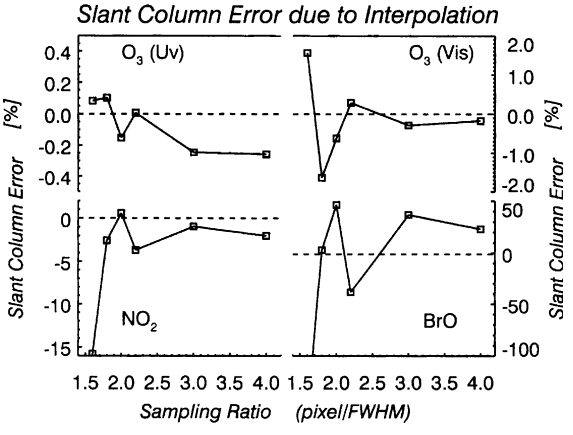

Fig. 6. Slant column errors due to spectral Doppler-shift interpolation patterns for fittings of O_3 in the UV (GOME-2 Channel 2, 325–335 nm) and visible (Channel 3, 450–497 nm), NO_2 (Channel 3, 425–450 nm), and BrO (Channel 2, 344–360 nm) relative to perfect fit slant columns plotted over sampling ratios between 1.6 (strongly under-sampled) and 4.0 (GOME-2 nominal spectral resolution matches a sampling ratio of about 2).

As solar irradiance and earthshine radiance measurements from space always suffer from the Doppler-shift, the spectral interpolation error is nevertheless more or less constant and can be relatively well simulated if the instrumental slit function is known accurately. Errors in slant columns can be strongly reduced by including the corresponding interpolation (under-sampling) error spectrum in the fitting procedure as is routinely the case for GOME (Chance, 1998; Slijkhuis et al., 1999).

For large slit width a loss of spectral information is the price for decreasing interpolation errors. Opening the entrance slit instead of defocussing, both leading to over-sampling, has the advantage to increase SNR, which is beneficial to trace gas column retrieval.

The nominal spectral resolution of GOME-2 in the spectral range 325–335 nm (O_3 fitting window) is slightly below 0.24 nm and for NO_2 (425–450 nm) slightly above 0.48 nm, which for both windows correspond to about 2 detector pixels and has been aimed at to decrease under-sampling errors observed for GOME (about 1.6 detector pixels FWHM).

Fig. 7 demonstrates the advantage of what is further-on called the "open-slit" approach: Broadening the width of the instrumental entrance slit increases the intensity of light passing into the instrument. The balance between the effects of gain in SNR as a direct consequence and, on the other hand, loss of spectral information due to broadening of the slit function has been investigated. The effect of pure loss of spectral information on trace gas slant column retrieval without a change in SNR by defocussing has also been studied.

SNR errors for NO_2 are shown as a function of the slit FWHM up to 1.92 nm (4 times the nominal spectral resolution) for four selected nadir scenarios. Errors increase with increasing FWHM when using defocussing

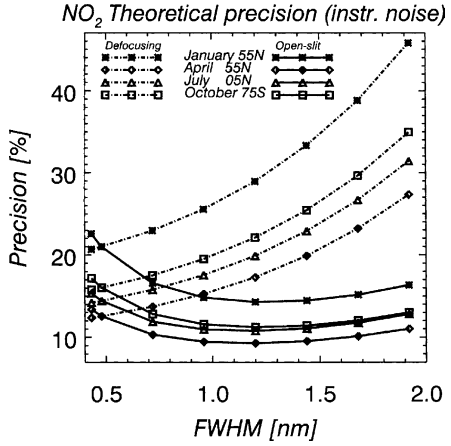

Fig. 7. SNR errors for fittings of NO_2 in the visible window between 425 and 450 nm, plotted over various FWHM of the slit function of up to 1.92 nm (4 times the nominal spectral resolution of about 0.48 nm for GOME-2 Channel 3). Four selected nadir scenarios have been considered.

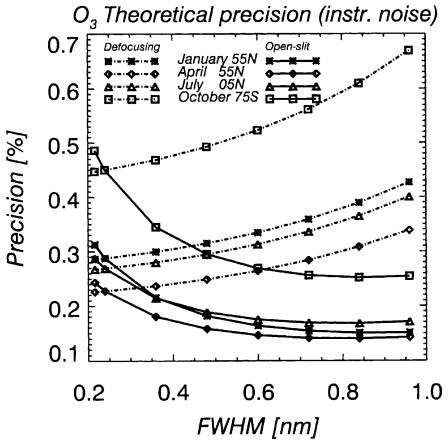

Fig. 8. Same as Fig. 7 for ozone fittings in the UV (GOME-2 Channel 2, 325–335 nm). Nominal spectral resolution is about 0.24 nm.

(no change in SNR). For the open-slit approach, the loss of spectral information due to decreased spectral resolution is more than over-compensated by the higher SNR. For all scenarios considered, the minimum error observed is at about 1.2 nm, i.e. 2.5 times the nominal spectral resolution.

For O_3 (Fig. 8) the relative effect of defocussing is smaller due to the much broader spectral characteristics of O_3 absorption. However, opening the slit leads also to a large gain. Minimum errors are achieved at about 0.84 nm, which is 3.5 times the nominal spectral resolution. Only at about 2 nm FWHM loss of spectral information is exactly compensated by gain in SNR, i.e. about the same errors occur as for the nominal case. The effect is similar for BrO (not shown).

5. Overall error budgets

Table 1 gives an overview of maximum and mean errors obtained for all error sources investigated in the error study (Kerridge et al., 2002). Light-shaded are errors which are on the same order of magnitude than the SNR errors. Significantly larger errors are dark-shaded. For O_3, the latter case appears quite often although errors are generally small in the UV fitting window. However, demands for O_3 retrievals are high and errors can add up significantly. For NO_2, one of the most significant error source is noise, which is therefore recommended to be specially treated, for instance by co-adding, which leads to a loss in spatial resolution. The most recommended option is to apply the open-slit approach.

Largest errors for NO_2 and other minor trace gases occur due to spectral characteristics of the aluminium diffuser plate, especially at low latitudes. The relative impact of the diffuser plate error decreases with increasing light paths and, thus, stronger absorption signatures; for high latitudes the effect is usually small. This has been investigated for GOME (Richter and Wagner, 2001), which uses the same diffuser material than currently designed for GOME-2. Monthly mean values for NO_2 from GOME over the equator show similar variations for 1996 and 1997, which are mainly related to the annual variation of the solar azimuth and elevation angle on the diffuser plate (Richter and Wagner, 2001).

6. Conclusions

The GOME-2 Error Assessment Study commissioned by EUMETSAT aimed at recommendations for operational settings for GOME-2 and other actions to mitigate errors focussing on GOME-2 instrument design and operation related issues. A subset of the results regarding trace gas column retrieval errors has been presented.

Errors for ozone are small and similar for all error sources considered. Large SNR errors arise for NO_2 and other minor trace gases at 0.1875 s integration time. One option for reducing these errors is co-adding, which is however, not favourable when looking at tropospheric retrievals through clouds. NO_2 and minor trace gas errors are severely dominated by diffuser plate signatures. BrO is additionally strongly affected by interpolation errors.

A significant improvement in trace gas slant column retrieval accuracies can be achieved by opening the slit by a factor of two. The slant column errors decrease significantly for NO_2 retrievals. Interpolation errors are strongly reduced. Further improvements in the spatial resolution could be achieved by further decreases in integration time. The current limit is 0.09375 s. However, it has to be emphasized that the technical feasibility of this option has not been analysed within this study. A change to a diffuser plate with spectral signatures of the order of 10^{-4} is recommended. A replacement with a quasi-volume-diffuser material is currently under investigation.

Acknowledgements

Thanks to ESA/ESTEC and the team at Rutherford Appleton Laboratoy for fruitful discussions. This work has been funded by EUMETSAT (EUMETSAT Contract No. EUM/CO/01/901/DK) and by the University and the State of Bremen.

References

Burrows, J., Weber, M., Buchwitz, M., et al. The Global Ozone Monitoring Experiment (GOME): Mission concept and first scientific results. J. Atmos. Sci. 56, 151–171, 1999a.

Burrows, J.P., Dehn, A., Deters, B., et al. Atmospheric remote-sensing reference data from GOME: part 1. temperature-dependent absorption cross-sections of NO_2 in the 231–794 nm range. J. Quantum Spectrosc. Radiat. Trans. 60, 1025–1031, 1998.

Burrows, J.P., Richter, A., Dehn, A., et al. Atmospheric remote-sensing reference data from GOME: part 2. temperature-dependent absorption cross-sections of O_3 in the 231–794 nm range. J. Quantum Spectrosc. Radiat. Trans. 61 (4), 509–517, 1999b.

Callies, J., Corpaccioli, E., Eisinger, M., et al. GOME-2 – METOP's second generation sensor for operational ozone monitoring. ESA Bulletin 102, 28–36, 2000.

Chance, K. Analysis of BrO measurements from the global ozone monitoring experiment. Geophys. Res. Lett. 25 (17), 3335–3338, 1998.

de Beek, R. SCIAMACHY Level 0-to-1 processor closed-loop tests, Technical Report, ESA/ESTEC, Envisat-1 Program, Contract 13594/99/NL/PR, 2002.

Eisinger, M. KVANT – a DOAS-type algorithm for the retrieval of trace gas vertical columns from atmospheric optical depth measurements. Institute of Environmental Physics, University of Bremen, Private communication, Available from: <http://www.iup.physik.uni-bremen.de/KVANT>, 1998.

Hartman, W., Aben, I., Siddans, R., et al. GOME-2 polarisation measurements. In: Proceedings of EUMETSAT Users Conference 2001, EUMETSAT, 2001.

Kerridge, B., Siddans, R., Latter, B., et al. Study – GOME-2 Error Assessment, Final Report Draft Version 1.1, EUMETSAT Contract EUM/CO/01/901/DK, EUMETSAT, Am Kavalleriesand 31, Postfach 100555, D-64295 Darmstadt, Germany, 2002.

Kurucz, L.R., Furenlid, I., Brault, J., et al. Solar flux atlas from 296 to 1300 nm, Technical Report, National Solar Observatory, Sunspot, New Mexico, 1984.

Platt, U., Perner, D. Direct measurement of atmospheric HCHO, HNO_2, O_3, NO_2 and SO_2 by differential optical absorption spectroscopy. J. Geophys. Res. 85, 1980.

Richter, A., Wagner, T. Diffuser plate spectral structures and their influence on GOME slant columns, Technical note Available from: <http://www.iup.physik.uni-bremen.de/gome/data/diffuser_gome.pdf>, IUP Bremen, IUP Heidelberg, 2001.

Roscoe, H.K., Fish, D.J., Jones, R.L. Interpolation errors in UV-visible spectroscopy for stratospheric sensing: implications for sensitivity, spectral resolution, and spectral range. Appl. Opt. 35, 427–432, 1996.

Rozanov, A., Rozanov, V., Burrows, J.P. A numerical radiative transfer model for a spherical planetary atmosphere: combined differential–integral approach involving the Picard iterative approximation. J. Quantum Spectrosc. Radiat. Trans. 69, 491–512, 2001.

Rozanov, V.V., Diebel, D., Spurr, R.J.D., et al. GOMETRAN: A radiative transfer model for the satellite project GOME, the plane-parallel version. J. Geophys. Res. 102 (D14), 16683–16695, 1997.

Slijkhuis, S., Bargen, A., Thomas, W., et al. Calculation of ''undersampling correction spectra'' for DOAS spectral fitting. In: ESAMS '99 – European Symposium on atmospheric Measurements from Space, ESA/ESTEC, vol. 2, Noordwijk, The Netherlands, pp. 563–569, 1999.

Vountas, M., Rozanov, V., Burrows, J. Ring effect: impact of rotational Raman scattering on radiative transfer in Earth's atmosphere. J. Quantum Spectrosc. Radiat. Trans. 60 (6), 943–961, 1998.